Effect of an electron-phonon interaction on the one-electron spectral weight of a *d*-wave superconductor

A. W. Sandvik,[1,2,*] D. J. Scalapino,[2,†] and N. E. Bickers[3,‡]
[1]*Department of Physics, Åbo Akademi University, Porthansgatan 3, FIN-20500 Turku, Finland*
[2]*Department of Physics, University of California, Santa Barbara, California 93106-9530, USA*
[3]*Department of Physics, University of Southern California, Los Angeles, California 90089-0484, USA*
(Received 5 September 2003; published 30 March 2004)

We analyze the effects of an electron-phonon interaction on the one-electron spectral weight $A(k,\omega)$ of a $d_{x^2-y^2}$ superconductor. We study the case of an Einstein phonon mode with various momentum-dependent electron-phonon couplings and compare the structure produced in $A(k,\omega)$ with that obtained from coupling to the magnetic π-resonant mode. We find that if the strength of the interactions are adjusted to give the same renormalization at the nodal point, the differences in $A(k,\omega)$ are generally small but possibly observable near $k=(\pi,0)$.

DOI: 10.1103/PhysRevB.69.094523 PACS number(s): 79.60.−i, 74.72.−h, 74.25.Kc

I. INTRODUCTION

The role of the electron-phonon coupling in the high T_c cuprates remains a puzzle. The initial finding of the absence of a phonon signature in the temperature dependence of the resistivity[1] and the small size of the isotope effect in the optimally doped cuprates[2] suggested that the electron-phonon interaction played a relatively unimportant role in these strongly-correlated materials. However, large isotope effects away from optimal doping,[2,3] significant phonon renormalization induced in the superconducting state,[4–7] and recent interpretations of angle-resolved photoemission spectroscopy (ARPES) data[8,9] continue to raise questions regarding the nature and role of the electron-phonon interaction in the high T_c cuprates.

One point of view is that the effects of the strong Coulomb interaction act to suppress the electron-phonon interaction and that while the electron-lattice interaction enters the problem, it does so on a secondary level coming along as it were for the ride. For example, in this view the large isotope effects observed in some of the cuprates away from optimal doping arises from the influence of the lattice on stripe fluctuations, acting to stabilize these and thus suppressing superconductivity.[10] Similarly, the superconductivity-induced phonon renormalization and the possible Engelsberg-Schrieffer[11] signature in the ARPES data could be interpreted as naturally occurring in an interacting system but having little effect on the underlying superconducting pairing mechanism. Alternatively one might interpret the isotope effect and the phonon renormalization as supporting the existence of a significant electron-phonon coupling. Furthermore, ARPES measurements have been specifically interpreted in terms of phonon modes that could drive $d_{x^2-y^2}$ pairing.[9] Here, we analyze a simple model of an electron-phonon interaction with the goal of obtaining insight into what one expects to see in the ARPES data of a $d_{x^2-y^2}$ superconductor with electron-phonon interactions.

Continuing technological advances along with improved sample quality have allowed ARPES to probe details of the energy and momentum structure of the one-electron excitations in the cuprate materials.[12] Although simplified, the sudden approximation leads to a useful picture in which the ARPES intensity is equal to the square of a matrix element which depends upon the photon energy, polarization, and the sample geometry times a product of the single-particle spectral weight

$$A(k,\omega)=\frac{1}{\pi}\mathrm{Im}\{G(k,\omega)\} \tag{1}$$

and a Fermi factor $f(\omega)$. Here $G(k,\omega)$ is the one-electron Green's function. Thus, the idea is that from the k and ω dependence of the ARPES data, one can extract information about the spectral weight $A(k,\omega)$. Then, from this, one seeks to learn about the electron self-energy $\Sigma(k,\omega)$ and the structure of the effective interaction. In particular, the role of spin fluctuations and the π resonance on the superconducting state spectral function have been studied.[13–15] With the recent suggestions[8] from ARPES measurements that there may be a significant coupling of the electrons to a phonon with an energy of order 40 meV, one would like to understand how this would effect the ARPES spectrum.

From the number of atoms in a unit cell, it is clear that there are a large number of phonon modes in the cuprates. Here we will focus on several of the modes associated with the motion of the O ions. We will treat these as Einstein phonons. Then for a Hubbard-like model in which the Cu sites form the Hubbard lattice, the effective electron-electron interaction is

$$V(q,\omega)=\frac{2|g(q)|^2\Omega_0}{\omega^2-\Omega_0^2+i\delta}. \tag{2}$$

If $|g(q)|^2=|g|^2$ is independent of the momentum transfer, $V(q,\omega)$ does not couple to the $d_{x^2-y^2}$-pairing channel. This could model the coupling to the c-axis vibration of the apical oxygen. Alternatively, if the electron-phonon matrix element is momentum dependent, the interaction given by Eq. (2) can couple to the $d_{x^2-y^2}$-pairing channel.

The possibility that an electron-phonon interaction could give rise to d-wave pairing has been discussed by various

authors.[9,16–25] In one approach, the *d*-wave pairing interaction occurs as the result of the interplay of the O half-breathing mode and the exchange interaction.[9] Other approaches suggest that the Coulomb interaction can lead to a peaking of the electron-phonon coupling at small momentum transfers which favors $d_{x^2-y^2}$ pairing.[16–20] This type of momentum dependence also occurs directly for certain phonon modes. For example, for the Cu-O-Cu bucklinglike mode[21–25] the square of the electron-phonon coupling constant is

$$|g(q)|^2=|g|^2\left[\cos^2\left(\frac{q_x}{2}\right)+\cos^2\left(\frac{q_y}{2}\right)\right]. \tag{3}$$

Setting $q=k-k'$, the momentum-dependent part of this coupling factors into a sum of separable terms

$$|g(k-k')|^2=|g|^2[1+\tfrac{1}{4}(\cos k_x-\cos k_y)(\cos k'_x-\cos k'_y)+\cdots], \tag{4}$$

including additional $(\cos k_x+\cos k_y)$ and $(\sin k_x\pm\sin k_y)$ factors. The plus sign in front of the *d*-wave term implies that this type of phonon exchange provides an attractive channel for *d*-wave pairing. The key point is that if the electron-phonon coupling $|g(k,k')|$ falls off at large $|k-k'|$ momentum transfers, then such a phonon exchange can mediate *d*-wave pairing.

Alternatively, an in-plane O breathinglike mode has

$$|g(q)|^2=|g|^2\left[\sin^2\left(\frac{q_x}{2}\right)+\sin^2\left(\frac{q_y}{2}\right)\right]. \tag{5}$$

This increases at large momentum transfers giving rise to a repulsive interaction in the $d_{x^2-y^2}$-channel. Setting $q=k-k'$ in Eq. (5) one finds that

$$|g(k-k')|^2=|g|^2[1-\tfrac{1}{4}(\cos k_x-\cos k_y)(\cos k'_x-\cos k'_y)+\cdots], \tag{6}$$

and the minus sign in the second term implies that this phonon suppresses *d*-wave pairing.

In Sec. II we discuss the simplified case of a cylindrical Fermi surface and a separable phonon mediated interaction. This provides insight into the differences between the *s*-wave and *d*-wave cases and establishes the structure of the singularities in the self-energy that are reflected in $A(k,\omega)$ for an Einstein mode. While in the actual materials, the singularities are broadened by the dispersion of the phonon mode, quasiparticle lifetime effects due to other interactions and impurities, as well as finite temperature effects, these results show the type of structure that can appear in $A(k,\omega)$ due to phonons. It also provides an example for which one can study the difference in $A(k,\omega)$ which occurs for modes that couple only to the normal *Z* part of the self-energy (such as the Holstein mode), only to the $d_{x^2-y^2}$ channel or to both. In Sec. III, we include the effects of a t-t' band structure and the momentum dependence of the coupling. We consider the three different electron-phonon coupling constants discussed above and compare these with the response to the π-resonance spin-fluctuation mode. The analysis of the π-resonance mode has been extensively discussed in Refs. 14,15. Section IV contains a summary of the results and our conclusions.

II. A CYLINDRICAL FERMI SURFACE AND AN EINSTEIN PHONON

In this section we consider the case of a cylindrical Fermi surface and an interaction arising from the exchange of an Einstein phonon of frequency Ω_0;

$$V(\theta,\theta',\omega)=\frac{2|g(\theta,\theta')|^2\Omega_0}{\omega^2-\Omega_0^2+i\delta}. \tag{7}$$

Here, θ and θ' denote different *k* vectors on the cylindrical Fermi surface. With Eq. (4) in mind, we will take $|g(\theta,\theta')|^2$ to have the separable form

$$|g(\theta,\theta')|^2=|g_z|^2+|g_\phi|^2\cos 2\theta\cos 2\theta'. \tag{8}$$

The one-electron Green's function can be written as

$$G(k,\omega)=\frac{Z(\omega)\omega+\epsilon_k}{(Z(\omega)\,\omega)^2-\epsilon_k^2-\phi^2(\theta,\omega)}, \tag{9}$$

with $\epsilon_k=k^2/2m-\mu$, the renormalization parameter $Z(\omega)$, and the gap parameter $\phi(\theta,\omega)=\phi(\omega)\cos(2\theta)$. The Eliashberg equations for $Z(\omega)$ and $\phi(\omega)$ are

$$[1-Z(\omega)]\omega=\lambda_z\frac{\Omega_0}{2}\int_0^\infty d\omega'\int\frac{d\theta}{2\pi}\times\mathrm{Re}\left\{\left(\frac{Z(\omega')\omega'}{\{[(Z(\omega')\,\omega']^2-\phi^2(\omega')\cos^2 2\theta\}^{1/2}}\right)\times\left(\frac{1}{\omega'+\omega+\Omega_0-i\,\delta}-\frac{1}{\omega'-\omega+\Omega_0-i\,\delta}\right)\right\} \tag{10a}$$

$$\phi(\omega)=\lambda_\phi\frac{\Omega_0}{2}\int_0^\infty d\omega'\int\frac{d\theta}{2\pi}\times\mathrm{Re}\left\{\left(\frac{\phi(\omega')\cos^2 2\theta}{\{[Z(\omega')\omega']^2-\phi^2(\omega')\cos^2 2\theta\}^{1/2}}\right)\times\left(\frac{1}{\omega'+\omega+\Omega_0-i\,\delta}+\frac{1}{\omega'-\omega+\Omega_0-i\,\delta}\right)\right\}, \tag{10b}$$

with $\lambda_z=2|g_q|^2N(0)/\Omega_0$ and $\lambda_\phi=2|g_\phi|^2N(0)/\Omega_0$. Here $N(0)$ is the one-electron density of states at the Fermi surface.

In order to determine the effect of the phonon on $Z(\omega)$ and $\phi(\omega)$, we will adapt an approximation used in the early studies of the role of phonons on the superconducting $I(V)$ characteristic.[26] From the form of Eq. (10), one sees that

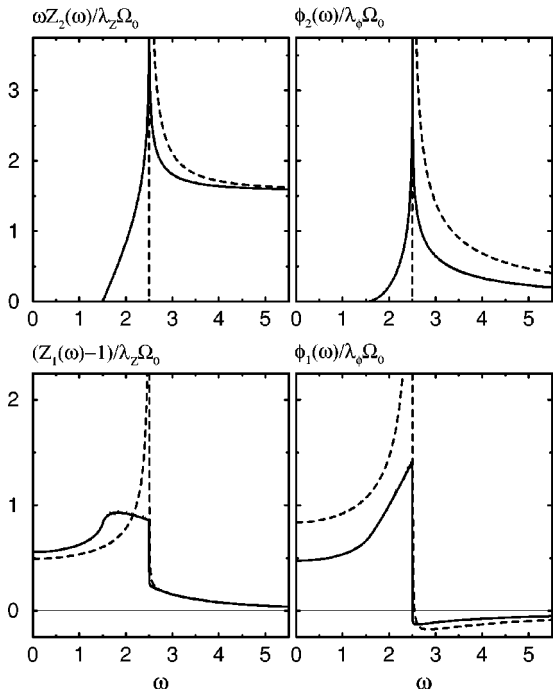

FIG. 1. Results for the real and imaginary phonon-induced contribution to $Z(\omega)$ and $\phi(\omega)$ for a *d*-wave (solid) and an *s*-wave (dashed) superconductor. Here we have taken a cylindrical Fermi surface and a separable interaction. $Z(\omega)$ and $\phi(\omega)$ are normalized with respect to the appropriate coupling constants. For the *s*-wave case, $\lambda_z=\lambda_\phi$. For all of the circular Fermi surface plots, energy is measured in units of Δ_0 and $\Omega_0=1.5\,\Delta_0$. With this normalization $\omega Z_2(\omega)/\lambda_z\Omega_0$ goes to $\pi/2$ as $\omega\to\infty$.

there will be structure in $Z(\omega)$ and $\phi(\omega)$ when $\omega\simeq\pm(\Omega_0+\Delta(\theta))$. In this case, ω' will be of order the gap $\Delta(\theta)$ at the gap edge

$$\Delta(\theta)=\frac{\phi[\theta,\omega=\Delta(\theta)]}{Z[\theta,\omega=\Delta(\theta)]}. \tag{11}$$

Therefore, if the low-energy response in the superconducting state is well described in terms of BCS *d* wave quasiparticles, one can replace $Z(\omega')$ and $\phi(\theta,\omega')/Z(\omega')$ inside the integrals by $Z(0)$ and $\Delta(\theta)=\Delta_0\cos 2\theta$. Then, taking the imaginary parts of Eq. (10), we have for $\omega>0$

$$\omega Z_2(\omega)=2\lambda_z\Omega_0\int_{\theta_c}^{\pi/4}\frac{(\omega-\Omega_0)d\theta}{[(\omega-\Omega_0)^2-\Delta_0^2\cos^2 2\theta]^{1/2}}, \tag{12a}$$

$$\phi_2(\omega)=2\lambda_\phi\Omega_0\int_{\theta_c}^{\pi/4}\frac{\Delta_0\cos^2 2\theta d\theta}{[(\omega-\Omega_0)^2-\Delta_0^2\cos^2 2\theta]^{1/2}}. \tag{12b}$$

Here θ_c is such that $\Delta(\theta_c)=\omega-\Omega_0$ and $\phi_2(\omega)$ and $Z_2(\omega)$ are even functions of ω for a time-ordered zero temperature Green's function.

Results for $\omega Z_2(\omega)$ and $\phi_2(\omega)$ are shown in the top panel of Fig. 1 for both a $d_{x^2-y^2}$-wave and a *s*-wave gap with $\Omega_0=1.5\Delta_0$. For a *s*-wave gap, $\cos 2\theta$ is set to 1 and $\theta_c=0$ in

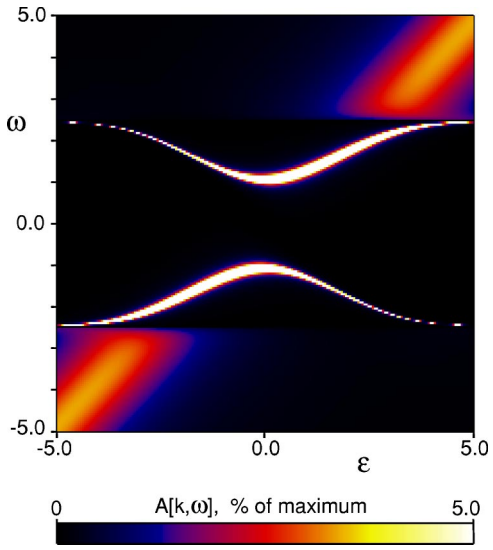

FIG. 2. (Color online) An intensity plot of the spectral weight $A(k,\omega)$ for the case of an *s*-wave superconductor coupled to a phonon with frequency Ω_0. As indicated on the color scale, the figure is "overexposed," i.e., features exceeding 5% of the maximum intensity appear white, in order to show the weaker features.

Eqs. (12a) and (12b). For the *s*-wave case, the imaginary parts of $Z(\omega)$ and $\phi(\omega)$ onset when ω exceeds $\pm(\Omega_0+\Delta_0)$ and exhibit a square-root singularity. For a $d_{x^2-y^2}$-gap, these functions onset linearly at $\omega=\pm\Omega_0$ because of the gap nodes and there is a log singularity at $\pm(\Omega_0+\Delta_0)$. The real parts of $Z(\omega)$ and $\phi(\omega)$ are obtained from the usual dispersion relations, and results for $Z_1(\omega)$ and $\phi_1(\omega)$ are shown in the lower panel of Fig. 1. For the *s*-wave case, ϕ_1 and Z_1 exhibit square-root singularities as ω approaches $\pm(\Omega_0+\Delta_0)$. This is just the expected Kramers-Kronig transform of the square-root singularity in ϕ_2 and Z_2. Similarly, the results for ϕ_1 and Z_1 for the $d_{x^2-y^2}$ case exhibit step discontinuities at $\omega=\pm(\Omega_0+\Delta_0)$ arising from the log singularities in ϕ_2 and Z_2. Naturally in real materials, phonon dispersion, impurity scattering, and finite-temperature effects broaden these features. Nevertheless, they provide a simple framework for analyzing the ARPES data.

An intensity plot of $A(k,\omega)$ for the case of an *s*-wave gap is shown in Fig. 2. Here, $A(k,\omega)$ is obtained from the imaginary part of $G(k,\omega)$, using the *s*-wave results for $Z(\omega)$ and $\phi(\omega)$ shown in Fig. 1 with $\lambda_z=\lambda_\phi=0.5$. The real part of the gap function is supplemented by an additional contribution from an underlying pairing interaction so that the magnitude of the gap at the gap edge is equal to Δ_0. Results for both the ARPES accessible region $\omega\leqslant 0$ and the inverse photoemission region $\omega>0$ are shown. The shift of spectral weight due to the quasiparticle coherence factors $\frac{1}{2}(1+\epsilon_k/E_k)$ is clearly seen as is the Engelsberg-Schrieffer signature showing the asymptotic approach of a peak in the spectral function to $\pm(\Omega_0+\Delta_0)$. Because of the square-root singularity in Z and ϕ, the asymptotic approach of this peak to $\pm(\Omega_0+\Delta_0)$ varies as $(\lambda\Omega_0/\epsilon_k)^2$. In addition,[27] the Fermi velocity is renormalized by $Z_1(\Delta_0)\approx 1.4$ so that the dispersion of the peak

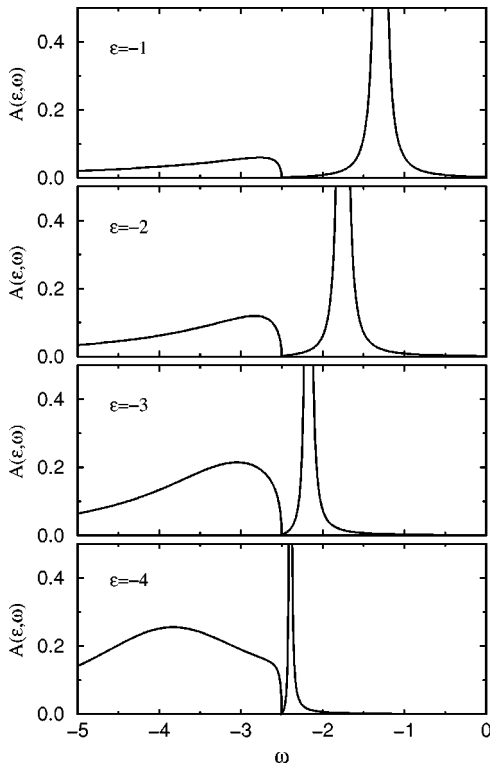

FIG. 3. Energy distribution curves showing $A(k,\omega)$ vs ω for various values of ϵ_k for an *s*-wave superconductor with $\lambda_z=0.5$. Here one sees that as ϵ_k exceeds $\Omega_0+\Delta_0=2.5$, a peak is left behind whose intensity weakens as ϵ_k increases. A Lorentzian broadening $\delta_\omega=0.025$ was used here and throughout the paper.

for ω near Δ_0 varies as $\sqrt{[\epsilon_k/Z_1(\Delta_0)]^2+\Delta_0^2}$ while for ω large compared to Ω_0, a broadened quasiparticle peak disperses as ϵ_k. Energy distribution curves (EDC) showing $A(k,\omega)$ versus ω for various values of ϵ_k are shown in Fig. 3 for $\omega\leqslant 0$. This is the type of EDC that one would expect to see for a traditional *s*-wave electron-phonon superconductor with a single dominant Einstein mode.[28] More generally, one would have multiple phonon modes and their dispersion along with possible finite temperature effects would lead to a richer response.

Intensity plots of $A(k,\omega)$ for the case of a $d_{x^2-y^2}$ gap are shown in Fig. 4. Just as for the *s*-wave case, $\phi_1(\theta,\omega)$ is supplemented so that the gap at the gap edge is $\Delta_0\cos 2\theta$. Figure 4(a) shows $A(k,\omega)$ for a cut along the antinodal direction in *k* space ($\theta=0$), while Fig. 4(b) shows the results for a cut along the nodal direction ($\theta=\pi/4$). The antinodal cut resembles the *s*-wave case in the transfer of spectral weight as ϵ_k passes through the Fermi energy and the renormalization of the quasiparticle dispersion. However, the Engelsberg-Schrieffer signature no longer asymptotically approaches $\pm(\Omega_0+\Delta_0)$, but rather appears to be broadened and cut off. In the *s*-wave case, the broadening due to the electron-phonon interaction did not set in until $|\omega|$ exceeded $\Omega_0+\Delta_0$ leading to the long sweep of the peak which occurs for $|\omega|$ just below $(\Omega_0+\Delta_0)$. However, the nodal regions associated with a $d_{x^2-y^2}$ gap lead to a finite broadening when $|\omega|$ exceeds Ω_0. The onset of this broadening is seen clearly in Fig. 4.

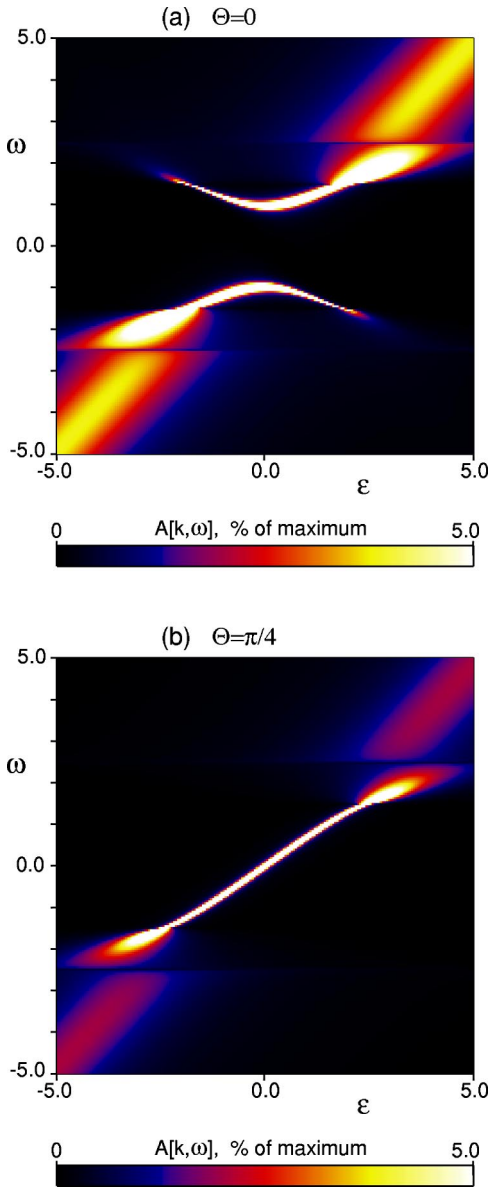

FIG. 4. (Color online) An intensity plot of $A(k,\omega)$ for a *d*-wave gap. Results for a $\theta=0$ cut are shown in (a) and for $\theta=\pi/4$ in (b), a nodal cut.

As we will discuss, termination of this peak is a reflection of the fact that for a $d_{x^2-y^2}$ gap, Z_1 and ϕ_1 have step discontinuities at $\pm(\Omega_0+\Delta_0)$ rather than the square-root singularities associated with an *s*-wave gap.

The nodal cut, shown in Fig. 4(b), appears on first glance to be similar to what one would expect for the normal state. That is, a renormalized $\epsilon_k/Z_1(k,0)$ dispersion for $\omega\ll\Omega_0$ with the dispersion returning to its band value ϵ_k for $\omega\gg\Omega_0$. However, the cutoff Engelsberg-Schrieffer signature still occurs for $|\omega|=\Omega_0+\Delta_0$. Thus, the full antinodal gap Δ_0 enters as the characteristic kink energy for all momentum slices. This simply reflects the $|\omega|=\Omega_0+\Delta_0$ singularities in Z and ϕ shown in Fig. 1. Again, the broadening of the Engelsberg-Schrieffer peak when $|\omega|$ exceeds Ω_0 is clearly seen in Fig. 4(b). In Fig. 5(a), various EDC slices of $A(k,\omega)$ are shown for the $d_{x^2-y^2}$ case. Comparing these with the

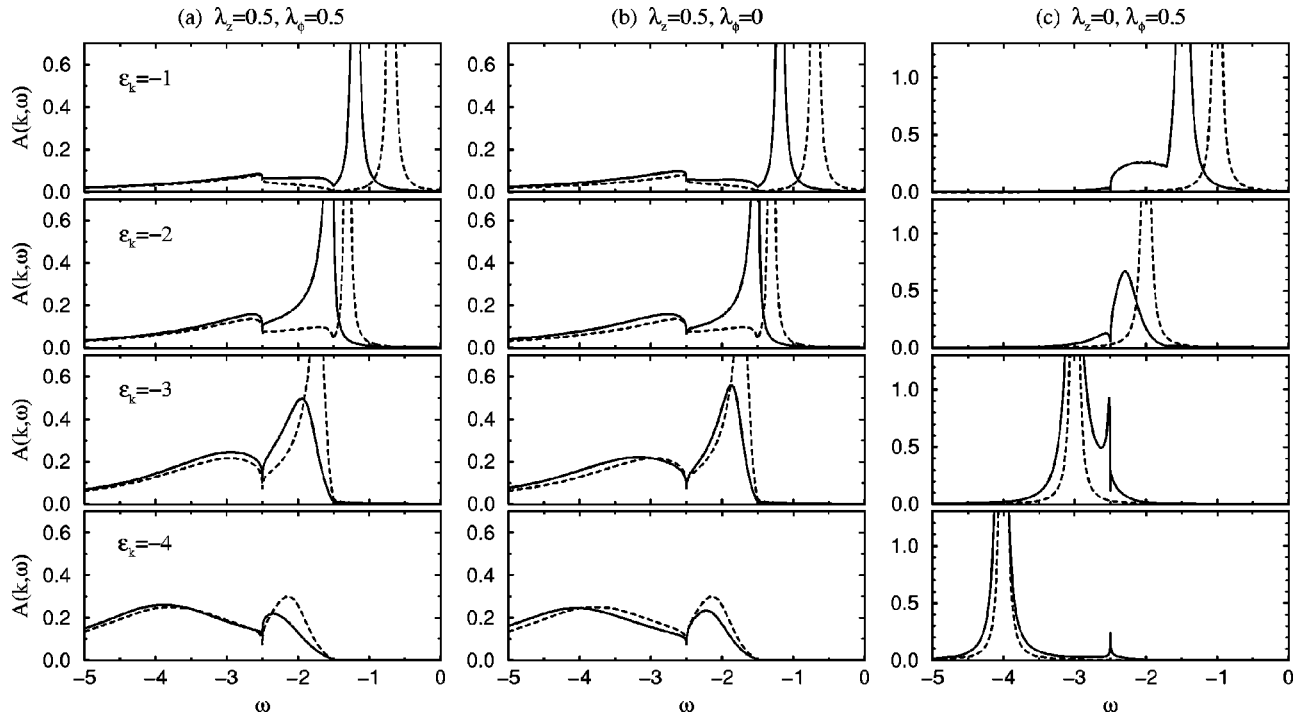

FIG. 5. Energy distribution curves (EDC) showing $A(k,\omega)$ vs ω for different values of ϵ_k ($-1,-2,-3,-4$ from top) with (a) $\lambda_z=\lambda_\phi=0.5$, (b) $\lambda_z=0.5,\lambda_\phi=0.0$, and (c) $\lambda_z=0.0,\lambda_\phi=0.5$. Results for the $\theta=0$ cut are shown as the solid curves and for $\theta=\pi/4$ as the dashed curves.

s-wave case, one sees the broadening and truncation of the Engelsberg-Schrieffer lower peak.

The difference in the structure of the Engelsberg-Schrieffer signature between the *s* and the $d_{x^2-y^2}$ cases can be understood from the plots of

$$\epsilon_k = -\sqrt{[Z_1(\omega)\omega]^2 - \phi_1^2(\omega)} \tag{13}$$

shown in Fig. 6. One can see that as one probes ϵ_k states which are further below the Fermi energy, two solutions of Eq. (13) develop. For the *s*-wave case shown in the upper panel of Fig. 6, an undamped lower-energy branch asymptotically approaches $\omega=-(\Omega_0+\Delta_0)$, and a second quasiparticle branch at $\omega\simeq-\epsilon_k$ evolves which is damped by the imaginary parts of Z and ϕ. As we have seen, these branches are reflected in the structure of $A(k,\omega)$ and the lower-energy branch represents the characteristic Engelsberg-Schrieffer signature for an *s*-wave superconductor. Similar plots for the $d_{x^2-y^2}$-case with $\theta=0$ and $\theta=\pi/4$ are shown in the lower panel of Fig. 6. Here, unlike the *s*-wave case, the low-energy branch is terminated, reflecting the fact that the singularities in Z_1 and ϕ_1 for the *d*-wave case are simply step discontinuities at $\pm(\Omega_0+\Delta_0)$. The onset of damping processes for the $d_{x^2-y^2}$ case when $\omega<-\Omega_0$ give rise to the discontinuity in slope seen at $\omega=-\Omega_0$.

Finally, for the *d*-wave case, the interaction may also have different λ_z and λ_ϕ coupling strengths. For example, the Holstein coupling has $\lambda_\phi=0$. Fig. 5(b) shows EDC slices of $A(k,\omega)$ for $\lambda_z=0.5$ and $\lambda_\phi=0$. For $\theta=\pi/4$, the gap vanishes and the results are identical to Fig. 5(a) for $\lambda_z=\lambda_\phi=0.5$. Even for $\theta=0$, the spectral weight for ($\lambda_z=0.5,\lambda_\phi=0$) is seen to be quite similar to the isotropic ($\lambda_z=0.5,\lambda_\phi=0$) case. Part of this arises from the fact that in both cases the gap has been set to Δ_0 at $\theta=0$. Fig. 5(c) shows $A(k,\omega)$ for the alternate limiting case in which the mode is coupled only to the $d_{x^2-y^2}$ channel ($\lambda_z=0,\lambda_\phi=0.5$). In this case, one sees a clear difference with respect to the isotropic case shown in Fig. 5(a). In particular, since $Z=1$, along $\theta=\pi/4$ where the gap vanishes, $A(k,\omega)$ is equal to its noninteracting form. That is, the Ω_0 mode does not effect $A(k,\omega)$ for $\theta=\pi/4$ if $\lambda_z=0$. These results show that, in principle, one can obtain information on the couplings of the mode to the normal Z part of the self-energy and the $d_{x^2-y^2}$ channels by examining $A(k,\omega)$ in the nodal and antinodal directions. However, in general, the effects are subtle.

III. BAND STRUCTURE AND THE EFFECT OF A MOMENTUM-DEPENDENT COUPLING

We turn next to the effects of the band structure and to the momentum dependence of the electron-phonon coupling. For the band structure, consider a square lattice with a nearest-neighbor hopping t and a next-nearest-neighbor hopping t'. In this case

$$\epsilon_k = -2t(\cos k_x + \cos k_y) - 4t' \cos k_x \cos k_y - \mu. \tag{14}$$

For $t'/t=-0.3$ and $\mu/t=-1$, one has the typical Fermi surface shown in Fig. 7 and the single spin electron density of states shown in the inset. We take the gap to be

$$\Delta_k = \Delta_0(\cos k_x - \cos k_y)/2. \tag{15}$$

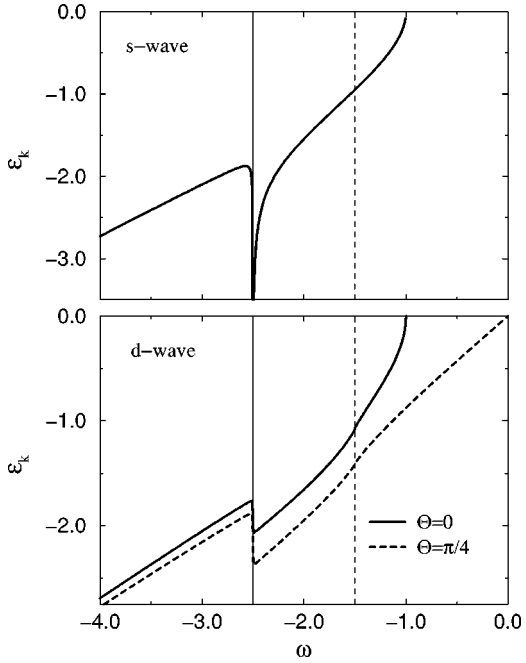

FIG. 6. Plots of $\epsilon_k = -\sqrt{[Z_1(\omega)\omega]^2 - \phi_1^2(\omega,\theta)}$ vs ω along the negative ω axis for $\lambda_\alpha = 0.5$ show the structure of the Engelsberg-Schrieffer signature. The upper panel is for an *s*-wave gap and the lower panel is for a *d*-wave gap with $\theta = 0$ shown as the solid curve and $\theta = \pi/4$ as the dashed curve.

In this case, the one-electron Green's function can be written in the form

$$G(k,\omega) = \frac{Z(k,\omega)\omega + [\epsilon_k + X(k,\omega)]}{[Z(k,\omega)\omega]^2 - [\epsilon_k + X(k,\omega)]^2 - \phi^2(k,\omega)}. \tag{16}$$

Adopting the same approximation as before, the phonon-induced contributions to the imaginary parts of the renormalization, energy shift, and gap parameters are given by

$$\omega Z_2(k,\omega) = \frac{\pi}{2N}\sum_{k'} |g(k-k')|^2 [\delta(E_{k'} + \Omega_0 - \omega) - \delta(E_{k'} + \Omega_0 + \omega)], \tag{17a}$$

$$X_2(k,\omega) = -\frac{\pi}{N}\sum_{k'} |g(k-k')|^2 \frac{\epsilon_{k'}}{2E_{k'}} \times [\delta(E_{k'} + \Omega_0 - \omega) + \delta(E_{k'} + \Omega_0 + \omega)], \tag{17b}$$

$$\phi_2(k,\omega) = \frac{\pi}{N}\sum_{k'} |g(k-k')|^2 \frac{\Delta_{k'}}{2E_{k'}} \times [\delta(E_{k'} + \Omega_0 - \omega) + \delta(E_{k'} + \Omega_0 + \omega)]. \tag{17c}$$

Here, as before, we assume that an underlying pairing interaction, most likely spin fluctuations, gives rise to a zero temperature $d_{x^2-y^2}$ superconducting state. At low energies this state is characterized by a renormalized band structure, Eq. (14), and chemical potential, a renormalized coupling constant $g(q)$, and a gap given by Eq. (15). These parameters have been used in the Eliashberg equations to describe the state which enters when an excitation at energy $\omega > \Omega_0$ decays to a lower energy $E_{k'}$ state (or when $\omega < -\Omega_0$ decays to $-E_{k'}$). The real parts of $Z(k,\omega)$, $\phi(k,\omega)$, and $X(k,\omega)$ are again found from the Kramers-Kronig dispersion relation. The spectral weight $A(k,\omega)$ is then obtained from Eq. (1) with the chemical potential shift removed from $X_1(k,\omega)$ and a contribution added to the real part of the gap so that the real part of the gap at the gap edge remains equal to Δ_k, Eq. (15). Note that the contributions of the underlying pairing interaction to Z and X, as well as the higher-energy part of ϕ, have not been included. Thus, there are additional renormalization and damping effects which do not appear. We basically are seeking to understand the leading contribution of the electron-phonon interaction which is superimposed on top of the other many-body interactions. This approach rests on the idea that in the superconducting state the low-lying electronic states are well described by BCS $d_{x^2-y^2}$-excitations[29] with renormalized band parameters t, t', and μ, a $d_{x^2-y^2}$-wave gap Δ_k, and renormalized electron-phonon coupling constants. Note, that here we are not taking into account the possible change in q dependence of the electron-phonon couplings produced for example by the Hubbard U.[16–20]

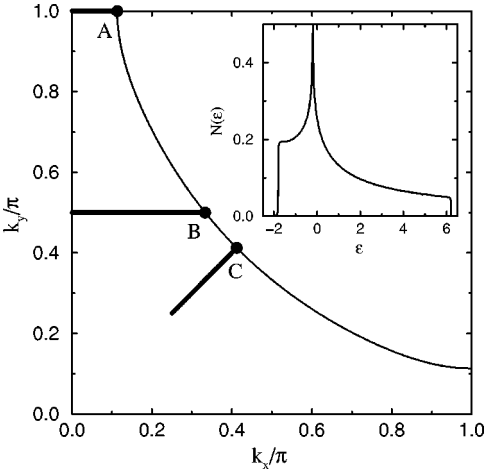

FIG. 7. The Fermi surface for $t'/t = -0.3$ and $\mu = -1$. The inset shows the single spin electron density of states. We will discuss the spectral weight for the cuts marked *A*, *B*, and *C*.

We begin by looking at the self-energy terms for the case of the buckling mode with $|g(q)|^2$ given by Eq. (3) and $|g|^2 = 0.5$ in units of t^{-2}. From Eq. (4), this value of $|g|^2$ corresponds to a *d* wave coupling strength coming from the buckling mode $\lambda_d \approx \frac{1}{4} 2|g|^2 N(0)/\Omega_0$ which is of order 0.1–0.2. Andersen *et al.*[30,31] have estimated that the total λ_d electron-phonon coupling is of order 0.3 and they find that the buckling mode gives the dominant part of this coupling. Results for $\phi(\omega,k)$, $Z(\omega,k)$, and $X(\omega,k)$ are shown in Fig. 8 for k at point *A* shown in Fig. 7. The imaginary parts of Z and ϕ exhibit the expected log singularity at $\Delta_0 + \Omega_0$ that we

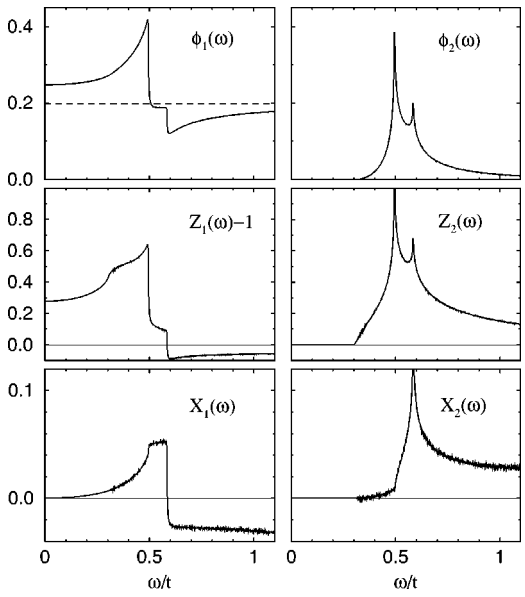

FIG. 8. The self-energy parameters ϕ, Z, and X vs ω for the case of the buckling phonon coupling, Eq. (3), with $\mathbf{k}=\mathbf{k}_A$ corresponding to the point A of Fig. 7. Here $|g|^2=0.5$.

previously saw for the case of a circular Fermi surface. In addition, there is a second log singularity at $E(0,\pi)+\Omega_0$ with $E(0,\pi)=\sqrt{\epsilon^2(0,\pi)+\Delta_0^2}$ which comes from the Van Hove singularity[14] at $k=(0,\pi)$. These log singularities in Z_2 and ϕ_2 manifest themselves via the Kramers-Kronig dispersion relation as step-down discontinuities in Z_1 and ϕ_1, as seen in Fig. 8. The energy shift parameter X has only the Van Hove singularity. Naturally, the dispersion of the phonon mode as well as finite temperature and lifetime effects will broaden these features in the actual system. The energy distribution of the spectral weight $A(k,\omega)$ for the buckling mode at momentum k_A is plotted in Fig. 9. It shows the quasiparticle peak at the gap edge Δ_{k_A} as well as structure

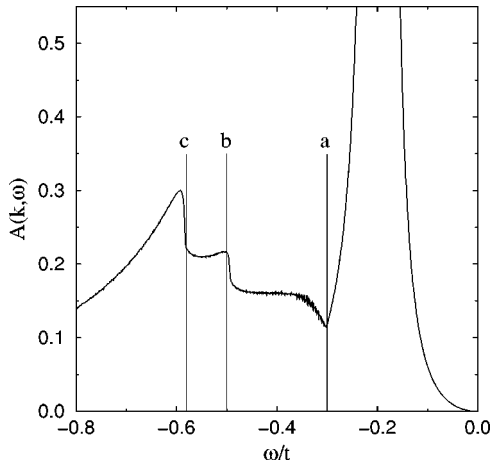

FIG. 9. $A(k,\omega)$ vs ω at $\mathbf{k}=\mathbf{k}_A$ for the case of a buckling mode with $|g|^2=0.5$. With energy measured in units of t, the gap amplitude $\Delta_0=0.2$, and the phonon energy $\Omega_0=0.3$. The vertical lines *a*, *b*, and *c* mark the characteristic energies $-\Omega_0$, $-(\Omega_0+\Delta_0)$, and $-[\Omega_0+E(0,\pi)]$, respectively.

associated with the buckling phonon at $\Omega_0+\Delta_0$ and $\Omega_0+E(0,\pi)$.

As noted in the Introduction, one would like to determine whether the structure observed in the ARPES data is due to phonons or the π-resonance spin-fluctuation mode. Eschrig and Norman[14,15] have analyzed the effect of the π-resonance using a detailed tight binding fit of the band energy ϵ_k and a coupling to the π-resonant mode of frequency Ω_0 given by

$$|g(q)|^2=g_{SF}^2\frac{\chi_Q}{1+4\xi^2[\cos^2(q_x/2)+\cos^2(q_y/2)]}. \quad (18)$$

Here, we will use the $t-t'$ band structure of Eq. (14) with $t'/t=-0.3$ and $\mu=-1$, set $\pi\chi_Q=1$, $\xi=2$, and $g_{\mathrm{SF}}^2\chi_Q=5$. This corresponds to having $U/t\sim 4.6$ in an effective Hubbard random-phase approximations interaction. In addition, with this choice for g_{SF}^2 we will find that $Z_1(k_F,0)$ at the nodal point C is comparable with $Z_1(k_F,0)$ for the phonons. This makes it convenient for addressing the question of whether there are significant spectral differences due simply to the structure of the momentum-dependent couplings that would allow one to determine the nature of the mode from the ARPES data. Note that for the spin-fluctuation interaction with $|g(q)|^2$ given by Eq. (18), there is a minus sign on the right-hand side of Eq. (17c) for the gap parameter. So to summarize, for the three types of phonon couplings we take $|g|^2=0.5$ in units of t^{-2} which gives $Z_1(k_F,0)\simeq 1.3$. For the π-resonance mode coupling, setting $g_{SF}^2\chi_Q=5$ gives $Z_1(k_F,0)\simeq 1.3$.

Intensity plots of $A(k,\omega)$ for the constant Holstein coupling, the buckling mode coupling Eq. (3), the breathing mode coupling Eq. (5), and the π-resonance mode coupling Eq. (18), are shown in Fig. 10 for the momentum cut A. Similar intensity plots for the momentum cuts B and C are shown in Figs. 11 and 12. In Fig. 10, one sees a high-intensity quasiparticle peak and weaker structures onsetting at $\omega=-(\Omega_0+\Delta_0)$ and $-(\Omega_0+E(0,\pi)$ due to the coupling to the phonon or magnetic resonance modes. For the B momentum cut shown in Fig. 11, one can now move deep enough inside the Fermi sea that the Engelsberg-Schrieffer lower-energy peak (the upper bright curve in the figures) is broadened when ω becomes less than $-\Omega_0$ and terminated at a finite value of k_x as ω approaches $-(\Omega_0+\Delta_0)$. At still higher energies (ω more negative), a damped quasiparticle branch is seen. The nodal C cut is shown in Fig. 12. Here, one clearly sees the Engelsberg-Schrieffer signature with a quasiparticle peak which varies as $\epsilon_k/Z_1(k_F,0)$ near the Fermi surface, then disperses and bends as ω approaches $-(\Omega_0+\Delta_0)$. This peak is then terminated as a broadened high-energy quasiparticle branch appears at more negative values of ω.

The difference of $A(k,\omega)$ for the various modes is in fact subtle since all four have an Einstein spectrum with $\Omega_0=0.3t$, a $d_{x^2-y^2}$ gap with $\Delta_0=0.2t$, and a band structure with $t'/t=-0.3$ and $\mu=-1$. Thus, the characteristic energies Δ_0, $\Omega_0+\Delta_0$, and $\Omega_0+E(0,\pi)$ are the same. In addition as discussed, we have chosen the coupling constants so that $|g(q)|^2$ averaged over the Brillouin zone is the same for all

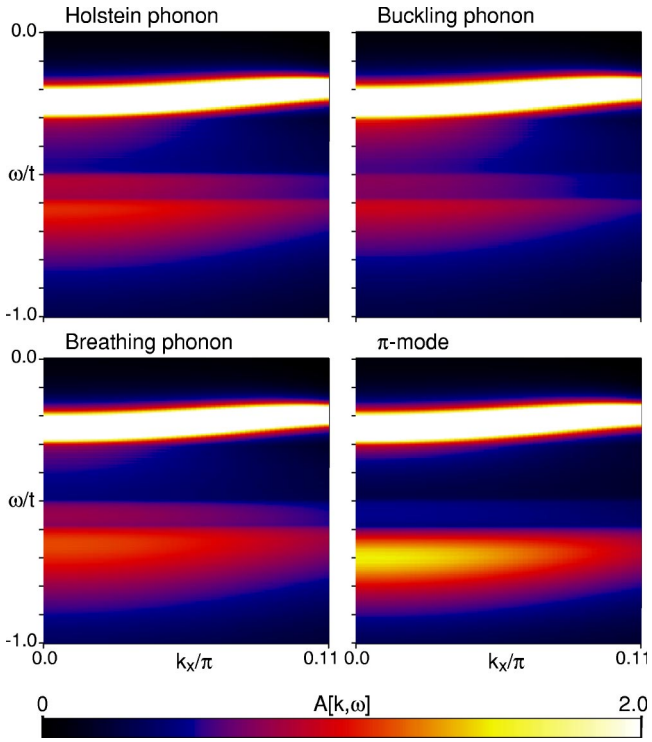

FIG. 10. (Color online) Intensity plots of $A(k,\omega)$ for the momentum cut A for four different couplings corresponding to the Holstein mode with $|g(q)|^2$ constant, the buckling mode Eq. (3), breathing mode Eq. (5), and π-resonance magnetic mode coupling Eq. (18). Here, $|g|^2=0.5$ and $g_{SF}^2\chi_Q=5$. The cutoff indicated on the color scale refers to the actual spectral weight intensity (as opposed to the relative scale used in the previous intensity plots) so that one can directly compare the effects of the different couplings.

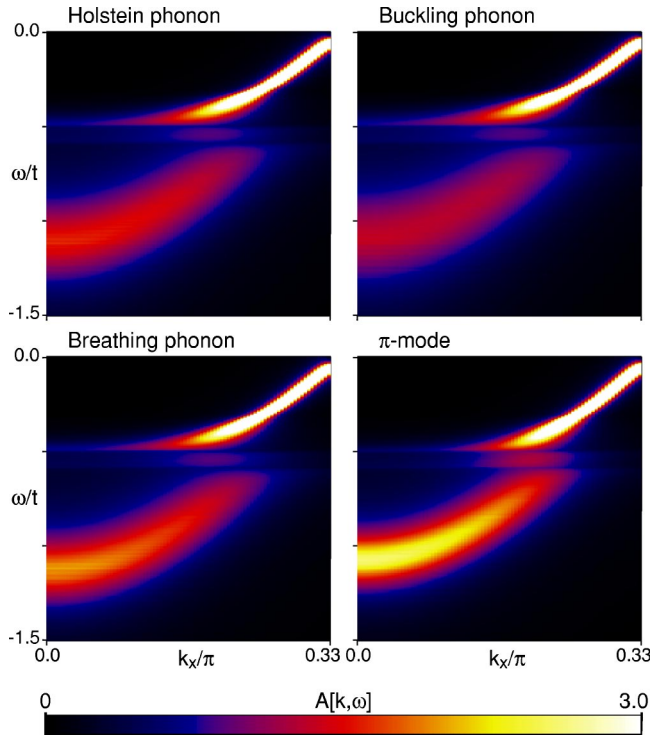

FIG. 11. (Color online) Intensity plots of $A(k,\omega)$ for the momentum cut B for the four different couplings.

four cases. Thus, the basic difference is the momentum structure of the different couplings shown in Fig. 13 for $q_x=q_y$. Here, we see that the spin-fluctuation resonant mode is clearly most strongly peaked at large momentum, followed by the breathing mode phonon, the uniform Holstein coupling, and lastly the buckling mode phonon which has $|g(\pi,\pi)|^2=0$. One consequence of the strong peak in the π mode coupling in the magnetic resonance mode coupling is seen in Fig. 10 for the A cut. Here, the increase of the intensity of the spectral weight $A(k,\omega)$ which occurs when ω decreases below $-[\Omega_0+E(\pi,0)]$ is greatest for the spin-fluctuation π resonance.

In Fig. 14 we show the energy distribution curves for the four modes for momentum $k=(0,\pi)$. $A(k,\omega)$ for all of the modes shows a strong peak at Δ_0. For the π mode, this is followed by a dip and then a secondary peak which develops as ω decreases below the Van Hove threshold at $-[\Omega_0+E(0,\pi)]$. It is this peak-dip-hump structure, for the case in which the effects of the bilayer splitting can be eliminated, that has been identified as a "fingerprint" of the π resonance.[14,15,32,33] Here, we see that indeed this structure is most pronounced for the π mode and smallest for the buckling mode. However, this is a quantitative effect rather than a qualitative one and if the phonon coupling increases at large momentum transfers, such as in the case of the breathing mode, this feature returns although not as strongly as for the π mode.

IV. CONCLUSIONS

It has been suggested,[34–36] that the structure in the ARPES data of BISCO is consistent with the existence of an

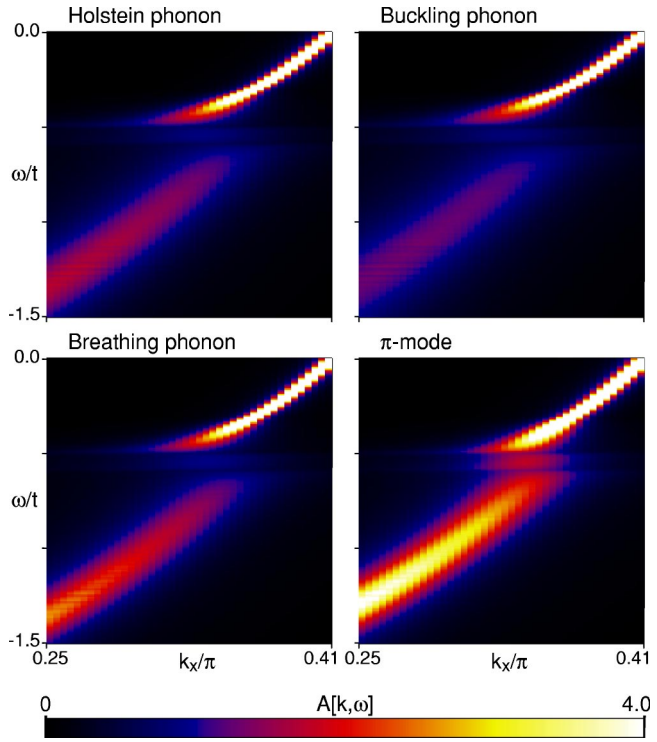

FIG. 12. (Color online) Intensity plots of $A(k,\omega)$ for the nodal momentum cut C for the four different couplings.

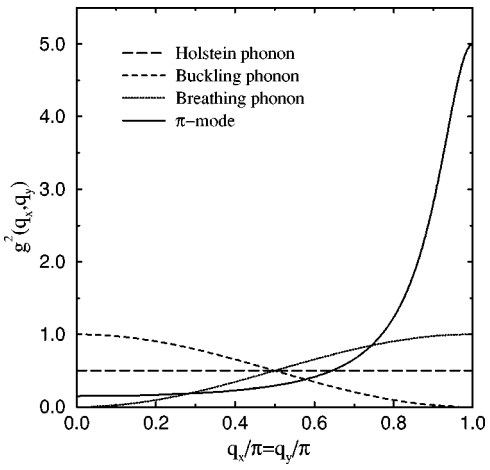

FIG. 13. The momentum dependence of the $|g(q)|^2$ coupling vs $q=q_x=q_y$ for the four different modes with $|g|^2=0.5$ for the phonon modes and $g_{SF}^2\chi_Q=5$ for the π-mode. Note that this is a slice of a two-dimensional (q_x,q_y) surface and that the volume enclosed by these surfaces is $(2\pi)^2|g|^2$ for each of these couplings.

Einstein-like mode with $\Omega_0\sim 40$ meV coupled to the electrons. Possible candidates for this mode are the magnetic resonance π-mode and various O phonon modes. As seen in Eq. (10), the coupling strength λ_z that determines the renormalization parameter Z comes from the *s* wave part of the effective interaction while the coupling λ_ϕ that determines the gap comes from the *d* wave part. Measurements of $A(k,\omega)$ with *k* along the nodal direction provide information on $Z(k,\omega)$ since $\Delta(k,\omega)=0$, while $A(k,\omega)$ measured near the antinodal region reflect structure due to both $Z(k,\omega)$ and $\Delta(k,\omega)$. Thus in principle, ARPES measurements offer the possibility for exploring both the *s*- and *d*-wave dependence of the interaction. However, from our results, it seems that it will be difficult to determine the origin of the mode based solely upon the momentum dependence of its coupling. This is because the forms of the couplings that we have studied have comparable coupling strengths and the spectral features at $\Omega_0+\Delta_0$ and $\Omega_0+E(0,\pi)$ arise generically from an Einstein mode coupled to quasiparticles with a *d*-wave gap and a band structure Van Hove singularity at $k=(0,\pi)$.

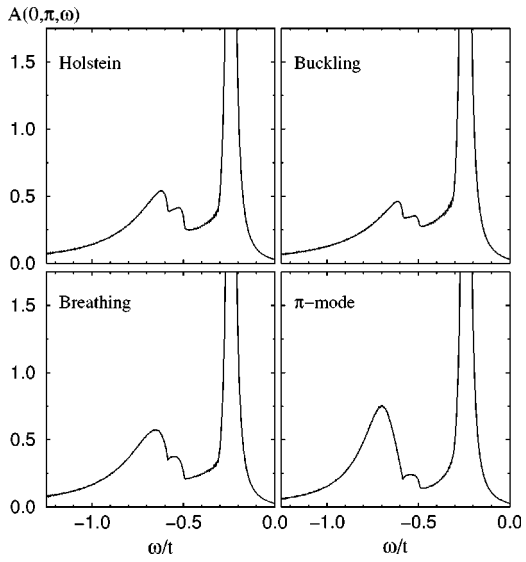

FIG. 14. Energy distribution curves (EDC) showing $A(k,\omega)$ vs ω at $k=(0,\pi)$ for the four different modes. A Lorentzian broadening $\delta_\omega=0.025$ was used. With a smaller δ_ω a dip at $\omega=\Omega_0$ also appears as in Fig. 9.

It would appear that the best place to look for a feature that could distinguish between, for example, the buckling phonon mode and the π-resonant mode is near the $k=(0,\pi)$ point. Here, the strong coupling of the π mode to the electrons for q near (π,π) leads to a secondary peak onsetting at an energy $\omega=-[E(0,\pi)+\Omega_0]$. For the buckling phonon mode, the coupling at $q=(\pi,\pi)$ vanishes and the response is weaker in the same frequency range. However, this is a quantitative rather than a qualitative effect. Furthermore, the observed peak-dip-hump structure could also be consistent with a coupling to the oxygen-breathing mode. Recently, it has been suggested that the q_z dependence for a bilayer system may identify the mode as having $q_z=\pi$, which would provide support for the π resonance.[37] However, further work on the odd and even bilayer phonon coupling is needed for comparison.

While the coupling to the π-resonance mode along with a higher-energy continuum spin-fluctuation spectrum provides an attractive unified framework, our results leave open the possibility that an oxygen-phonon mode could also play a role. As we have seen, even with a relatively modest electron-phonon coupling, one would expect to see evidence of some oxygen-phonon modes. If they are not seen, then this suggests that the strong Coulomb many-body effects act to suppress the electron-phonon coupling. Alternatively, if it can be shown that the π mode is not viable, oxygen-phonon modes could provide a source for the resonant mode features. The continuum spin fluctuations would, of course, also contribute in this mixed scenario. Here we should note that even if the mode were identified as the buckling mode, we find that its contribution to the magnitude of the $d_{x^2-y^2}$ gap is negligible because the increase in Z_1 more than offsets the increase in ϕ_1. Similar results for T_c were found by Nunner *et al.*[38] However, if the momentum dependence of the electron-phonon coupling were such that the effective λ_z was small compared with λ_ϕ, this would not be true.[39]

To conclude, we note that $A(k,\omega)$ for *k* along the nodal direction depends only on $Z(k,\omega)$ and $X(k,\omega)$, while if *k* is away from the nodal direction $\phi(k,\omega)$ enters. Thus, in principle, interactions which have significantly different λ_z and λ_ϕ coupling strengths should give rise to different interaction induced structures in $A(k,\omega)$ in the nodal and antinodal regions. However, for the couplings we have studied, it seems likely that the identification of the excitation responsible for the structure in the ARPES data will be decided on grounds other than the momentum dependence of the effective coupling. Naturally in some cases, the value of Ω_0 will provide a clear identification of the mode. In other cases, as noted, one may be able to use a symmetry-based argument.

One important aspect that remains under discussion is the strength of the various couplings. As we noted, LDA calculations[30,31] find intermediate values for the electron-phonon coupling. However, others have suggested that the electron-phonon coupling is stronger.[39,40] Likewise, there has

been a range of coupling strengths proposed for the π mode.[14,15,40–42] Here, there is general agreement regarding the relative size $I_0 = 0.035$ of the ratio of the spectral weight of the resonance per Cu to the total integrated spectral weight $g^2 S(S+1)/3 = 1$ per Cu in $Bi_2Sr_2CaCu_2O_{8+\delta}$.[43] However, there is disagreement[41,42] regarding whether the electron self-energy is effected by the smallness of I_0 and on the size of the coupling $(g_{SF}/t)^2$. Here, by varying ξ in Eq. (18), we have found that the size of I_0 directly effects the magnitude of the self-energy contribution arising from the interaction of the quasiparticle and the spin fluctuations. This is in agreement with the comments made in Ref. 41. However, we find our estimate of the coupling constant and the resulting size of the self-energy structures to be in reasonable agreement with Eschrig and Norman[14,15] and Ref. 42.

ACKNOWLEDGMENTS

We would like to thank Z.-X. Shen for discussing his data with us, for his physical insights, and his enthusiasm for this project. D.J.S. would also like to also acknowledge very useful discussions with S. V. Borisenko, W. Hanke, B. Keimer, and S. A. Kivelson. A.W.S. would like to acknowledge support from the Academy of Finland under Project No. 26175. D.J.S. acknowledges support from the National Science Foundation under Grant No. DMR02-11166.

*Electronic address: asandvik@abo.fi

†Electronic address: djs@vulcan2.physics.ucsb.edu

‡Electronic address: bickers@physics.usc.edu

[1] S. Martin, A.T. Fiory, R.M. Fleming, L.F. Schneemeyer, and J.V. Waszczak, Phys. Rev. B **41**, 846 (1990).

[2] J. P. Franck, in *Physical Properties of High T_c Superconductors IV*, edited by D. M. Ginsberg (World Scientific, Singapore, 1994), p. 189.

[3] M.K. Crawford, M.N. Kunchur, W.E. Farneth, E.M. McCarron, and S.J. Poon, Phys. Rev. B **41**, 282 (1990).

[4] C. Boulesteix, K. Hewitt, and J.C. Irwin, J. Phys.: Condens. Matter **12**, 9637 (2000).

[5] R.M. Macfarlane, H. Rosen, and H. Seki, Solid State Commun. **83**, 343 (1992).

[6] R.J. McQueeney, Y. Petrov, T. Egami, M. Yethiraj, G. Schirane, and Y. Endoh, Phys. Rev. Lett. **82**, 628 (1999).

[7] N. Pyka, W. Reichardt, L. Pintschovius, G. Engel, J. Rossat-Mignod, and J.Y. Henry, Phys. Rev. Lett. **70**, 1457 (1993).

[8] A. Lanzara, P.V. Bogdanov, X.J. Zhou, S.A. Keller, D.L. Feng, E.D. Lu, T. Yoshida, H. Eisaki, A. Fujimori, K. Kishio, J. Shimoyama, T. Noda, S. Uchida, Z. Hussain, and Z.-X. Shen, Nature (London) **412**, 510 (2001).

[9] Z.-X. Shen, A. Lanzara, S. Ishihara, and N. Nagaosa, Philos. Mag. B **82**, 1349 (2002).

[10] E. W. Carlson, V. J. Emery, S. A. Kivelson, and D. Orgad, in *The Physics of Conventional and Unconventional Supercoductors* edited by K. H. Bennemann and J. B. Ketterson (to be published by Springer-Verlag); cond-mat/0206217 (unpublished).

[11] S. Engelsberg and J.R. Schrieffer, Phys. Rev. **131**, 993 (1963).

[12] A. Damascelli, Z. Hussain, and Z.-X. Shen, Rev. Mod. Phys. **75**, 473 (2003).

[13] A. Kaminski, M. Randeria, J.C. Campuzano, M.R. Norman, H. Fretwell, J. Mesot, T. Sato, T. Takolashi, and K. Kadowaki, Phys. Rev. Lett. **86**, 1070 (2001).

[14] M. Eschrig and M.R. Norman, Phys. Rev. Lett. **85**, 3261 (2000).

[15] M. Eschrig and M.R. Norman, Phys. Rev. B **67**, 144503 (2003).

[16] M.L. Kulic and R. Zeyher, Phys. Rev. B **49**, 4395 (1994); R. Zeyher and M.L. Kulic, *ibid.* **53**, 2850 (1996).

[17] M. Grilli and C. Castellani, Phys. Rev. B **50**, 16 880 (1994).

[18] A.A. Abrikosov, Phys. Rev. B **52**, R15 738 (1995).

[19] G. Varelogiannis, Phys. Rev. B **57**, 13 743 (1998).

[20] Z.B. Huang, W. Hanke, E. Arrigoni, and D.J. Scalapino cond-mat/0306131 (unpublished). These Monte Carlo Calculations for a Hubbard model find that, while the electron-phonon vertex is suppressed at large momentum transfers, it can actually be enhanced at small momentum transfers.

[21] J. Song and J.F. Annett, Phys. Rev. B **51**, 3840 (1995); **52**, 6930(E) (1995).

[22] D.J. Scalapino, J. Phys. Chem. Solids **56**, 1669 (1995).

[23] A. Nazarenko and E. Dagotto, Phys. Rev. B **53**, R2987 (1996).

[24] T. Dahm, D. Manske, D. Fay, and L. Tewordt, Phys. Rev. B **54**, 12 006 (1996).

[25] N. Bulut and D.J. Scalapino, Phys. Rev. B **54**, 14 971 (1996).

[26] D.J. Scalapino and P.W. Anderson, Phys. Rev. **33**, A921 (1964).

[27] In the superconducting state the value of $Z_1(\Delta_0)$ is less than the normal state renormalization factor $1+\lambda = 1.5$ due to the additional energy associated with the gap. Traditionally, when Ω_0 was large compared to Δ_0, this effect was negligible. Here, however, since $\Omega_0 = 1.5\Delta_0$, the effective λ for the *s*-wave case is of order $2|g|^2 N(0)/(\Omega_0+\Delta_0) = 0.6\lambda = 0.3$. For the *d*-wave case, the effective λ is also reduced but not quite as much because of the nodes. In the following, we will use $Z_1(k, \omega = 0)$ at the nodal point to give the nodal Fermi velocity renormalization for the *d*-wave case.

[28] D. J. Scalapino, in *Superconductivity*, edited by R. D. Parks (Marcell Dekker, New York, 1969), Chap. 10.

[29] J.E. Hoffman, K. McElroy, D.-H. Lee, K.M. Lang, H. Eisaki, S. Uchida, and J.C. Davis, Science **295**, 466 (2002).

[30] O.K. Andersen, S.Y. Savrasov, O. Jepsen, and A.I. Liechtenstein, J. Low Temp. Phys. **105**, 285 (1996).

[31] O. Jepsen, O.K. Andersen, I. Dasgupta, and S. Savrasov, J. Phys. Chem. **59**, 1718 (1998).

[32] S.V. Borisenko, A.A. Kordyuk, T.K. Kim, A. Koitzsch, M. Knupfer, M.S. Golden, J. Fink, M. Eschrig, H. Berger, and R. Follath, Phys. Rev. Lett. **90**, 207001 (2003).

[33] T.K. Kim, A.A. Kordyuk, S.V. Borisenko, A. Koitzsch, M. Knupfer, H. Berger, and J. Fink, cond-mat/0303422 (unpublished).

[34] Z.-X. Shen and J.R. Schrieffer, Phys. Rev. Lett. **78**, 1771 (1997).

[35] M.R. Norman, H. Ding, J.C. Campuzano, T. Takeuchu, M. Randeria, T. Yokaya, T. Takakashi, T. Mochiku, and K. Kadowaki, Phys. Rev. Lett. **79**, 3506 (1997).

[36] M.R. Norman and H. Ding, Phys. Rev. B **57**, R11 089 (1998).

[37] M. Eschrig and M.R. Norman, Phys. Rev. Lett. **89**, 277005 (2002).

[38] T.S. Nunner, J. Schmalian, and K.H. Bennemann, Phys. Rev. B **59**, 8859 (1999).

[39] Recent calculations of the electron-phonon coupling to the B_1g mode find that the dominant coupling has $d_{x^2-y^2}$ symmetry (e.g., the leading constant term in Eq. (4) is suppressed] and is larger than the previous estimates of $\lambda \sim 0.1$ from Raman scat-

tering. This effects $A(k,\omega)$ near the antinodes and leads to significant $d_{x^2-y^2}$ pairing since it has a negligible contribution to the renormalization factor to Z (Private communication), T. P. Devereaux. For the Raman scattering experiments; see M. Opel, R. Hackl, T.P. Devereaux, A. Virosztek, A. Zawadowski, A. Erb, E. Walker, H. Berger, and L. Forro, Phys. Rev. B **60**, 9836 (1999).

[40] R. Zeyher and A. Greco, Phys. Rev. B **64**, 140510 (2001). These authors use an electron-phonon coupling $\lambda \sim 0.75$–1.0 and argue that the effective coupling of the electrons to the magnetic resonance mode g_{SF}^2 is significantly smaller than the coupling we have used. This work also differs from the present work in that the effect of $\phi_2(k,\omega)$ was not taken into account.

[41] H.-Y. Kee, S.A. Kivelson, and G. Aeppli, Phys. Rev. Lett. **88**, 257002 (2002).

[42] A. Abanov, A.V. Chubukov, M. Eschrig, M.R. Norman, and J. Schmalian, Phys. Rev. Lett. **89**, 177002 (2002).

[43] H.F. Fong, B. Bourges, Y. Sidis, L.P. Regnault, A. Ivanov, D.L. Milius, I.A. Aksay, and B. Keimer, Phys. Rev. B **61**, 14 773 (2000).